Photoactive systems based on semiconducting metal oxides

Photoactive Systems Based on Semiconducting Metal Oxides

1. Introduction

Among the materials employed in photocatalytic applications, transition metal-based semiconducting oxides play a paramount role. These materials are characterized by a band structure in which the valence band (VB), made up by the overlap of *2p* orbitals of O^{2-}, is fully occupied and the empty conduction band (CB), based on the *d* and *s* states of the metal ion, are energetically separated by a forbidden gap of some electron volt also called "band gap". [1] The systems employed in photocatalysis are usually n-type semiconductors. This physical property is due to the presence of intrinsic defects (such as vacancies) or chemical impurities that create shallow donor states whose electrons are easily thermalized in the conduction band. The well-established mechanism of heterogeneous photocatalysis depends on the electronic structure of the material and is based on the promotion of electrons from the VB to the CB occurring when photons of suitable energy impinge the solid. This phenomenon of charge separation implies the formation of mobile holes (h^+) in the valence band and mobile electrons (e^-) in the conduction band. The charge carriers that, moving in the crystal, reach the surface escaping recombination, are potentially capable to entail reductive (e^-) and oxidative (h^+) redox processes, respectively. The occurrence of a surface redox process depends, as a first approximation, on the interplay between the (electro)chemical potentials of the carriers in the bands and those of the redox pairs in the fluid phase in contact with the solid. Typical reductive processes are, for instance, the reduction of hydrogen ions to H_2 or that of carbon dioxide, both included in the challenging area of artificial photosynthesis. At variance, for reactions in the field of environmental photocatalysis, the main reduction process concern O_2 that forms superoxide ($O_2^{\bullet-}$), a typical Reactive Oxygen Species, or ROS, while the holes in valence band oxidize water molecules forming $OH^{\bullet}$ radicals, another oxidative ROS, able to mineralize

organic molecules present in various systems such as, for instance, wastewater [2-4], as sketched in Figure 1.

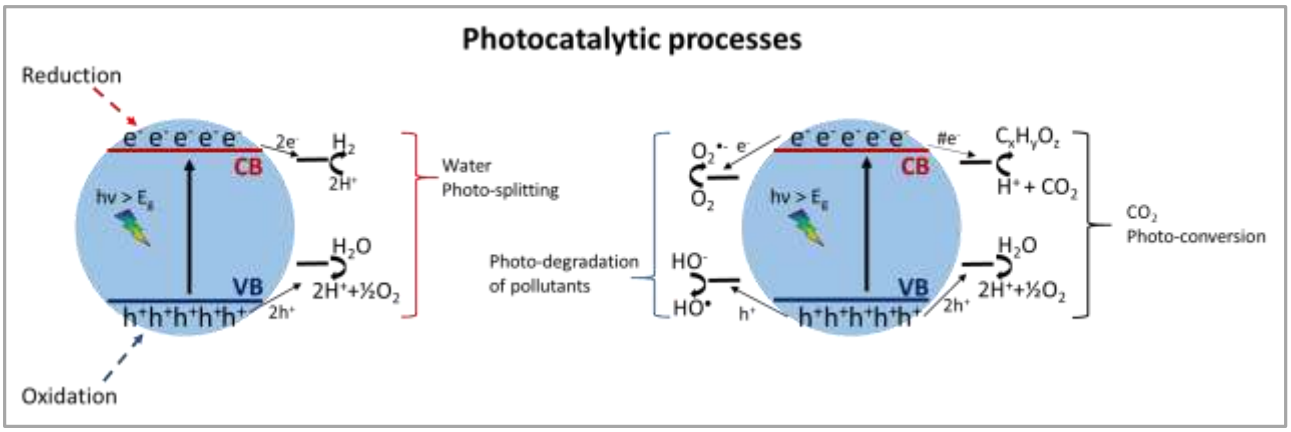

Figure 1: Schematic representation of charge carriers separation in a semiconductor and the possible photocatalytic reaction entailed.

The main factors limiting the performance of a heterogeneous photocatalyst based on a semiconducting oxide are two. The former is the recombination of charge carriers that limits the quantum yield of the process reducing the fraction of photonic energy converted in chemical energy. The second is related to the band gap amplitude of the solid. The most common semiconducting oxides for photocatalysis have, in fact, a band gap value corresponding to photons in the range of the ultraviolet radiation making necessary the use of these high energy photons in order to perform charge separation. This causes a severe problem for large scale applications aiming to use sunlight in photocatalysis since the fraction of UV photons in solar radiation at the earth surface is 5% only [5]. The obvious expedient of selecting photocatalysts with band gap corresponding to visible frequencies implicate, as a consequence, a net variation of the electrochemical potential of the bands compromising the redox ability of the system.

Different strategies have been developed to overcome this important shortcoming. The first one consists in engineering the electronic and optical properties of the oxide by doping, *i.e.* by the deliberate insertion of a foreign atom into the lattice, with formation of novel states inside the band gap, allowing charge separation with energy lower than the pristine material band gap. Figure 2 depicts how the doping procedure can modify the semiconductor energy gap for n-doped and p-doped

semiconductors, referred to the energy Fermi level (E_F, defined as the level at highest energy occupied at T = 0K).

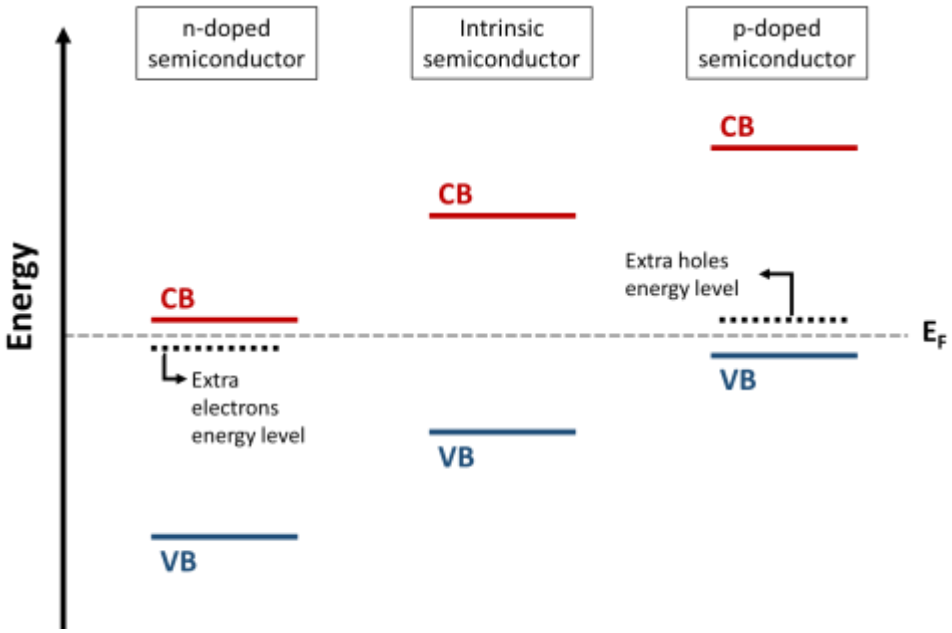

Figure 2: Schematic representation of the energy diagram change due to different doping procedure.

Another approach consists in coupling two distinct semiconductors with formation of active interfaces or heterojunctions. A heterojunction is defined as the surface of contact between two semiconductors resulting in a particular band alignment [6, 7] that depends on the band potentials and band widths of each semiconductor. Figure 3 reports three distinct cases of band alignment. The best performances have been observed in the case of *type-II* heterojunction, in which the band gaps of the two semiconductors are staggered. With this approach the charge carriers separation is improved since electrons and holes are stabilized on distinct materials, thus preventing direct recombination.

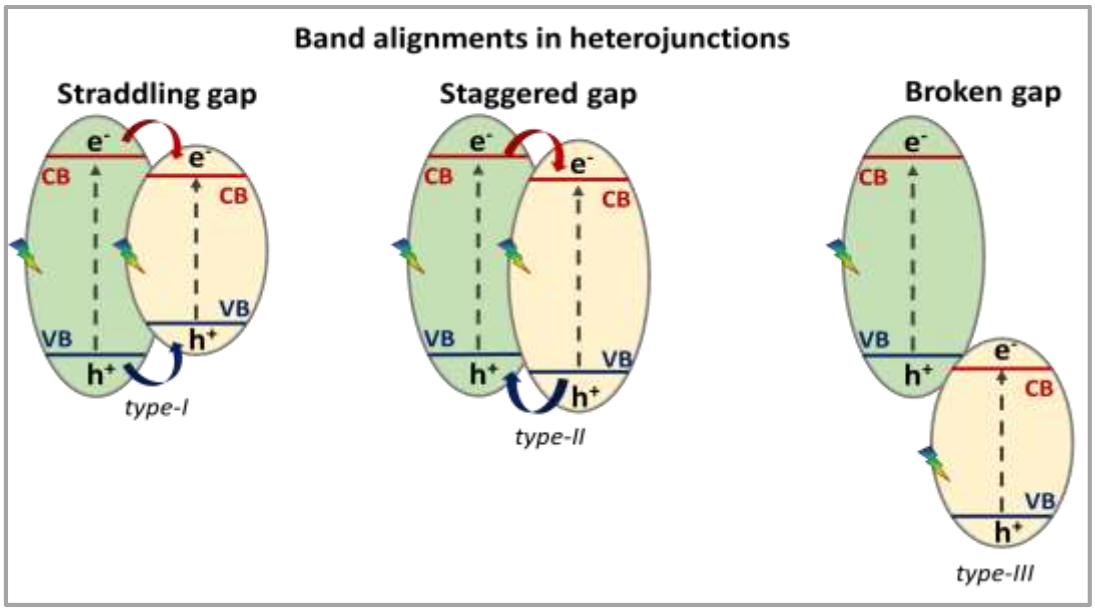

Figure 3: Schematic representation of the possible bands diagram occurring at semiconductor interfaces [6].

It has to be noticed, however, that in *type-II* heterojunctions (that is inspired to the Z-scheme of natural photosynthesis) the prospective redox ability of photogenerated carriers is attenuated since, after excitation, electrons move to a less negative potential and holes to a highest positive one (Figure 3, centre). Recently heterojunctions with a new type of scheme involving an alternative flow of the carriers at the interface has been developed, indicated as "direct Z-scheme or S-scheme" (Fig. 4).

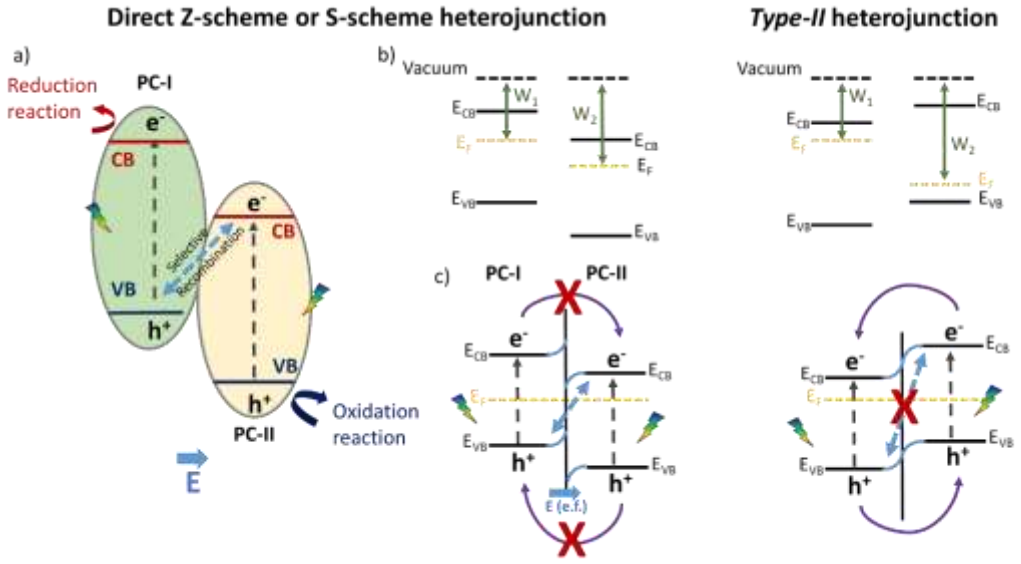

Figure 4: Interface charge carriers migration. Comparison between Direct Z-scheme or S-scheme and type-II heterojunction.

In this particular case, the bands are staggered as in the case of *Scheme II* but a particular work function (indicated as W_1 and W_2 in Fig. 4) of the two materials (indicated as PC-I and PC-II in Fig. 4) creates a peculiar electric field (displayed ad E in Fig. 4) at the interface causing the selective recombination of electrons and holes shown in Fig. 4. The spatial separation of the two photo-induced carriers is maintained but, differently from the case of *type-II* heterojunction, in this case the most favourable redox potentials present in the system are exploited [8, 9].

All the efforts to obtain novel and more efficient photocatalytic systems has to be accompanied by a deeper insight into the mechanisms of photocatalytic processes. To this aim the systematic use of advanced physical techniques of characterisation is mandatory. In this chapter we will illustrate the application of Electron Paramagnetic Resonance (EPR) in investigating the properties of photocatalytic materials active under irradiation of visible light. EPR is a particularly efficient technique in the characterisation of heterogeneous photocatalysts for more than one reasons. First, EPR is a quite sensitive technique allowing the detection of small amounts of paramagnetic entities. In photocatalytic phenomena, based on separation and reactivity of single charges carriers, such species bearing unpaired electrons are extremely common. Last but not least EPR has an additional feature consisting in the possibility of recording spectra in the dark or under illumination with frequencies typical of photocatalytic reactions (UV-vis) since there is no interference between the latter and the microwaves inducing magnetic resonance. This opportunity allows to investigate either the ground state or the excited states of the systems and also it makes possible to perform a sort of "operando" spectroscopy monitoring the state of the system during a photocatalytic process.

2. Photocatalytic phenomena explained via Electron Paramagnetic Resonance technique

When a metal oxide is irradiated with light having suitable energy, charge separation occurs in the solid, according to the following equation (1)

$$MeO_X + h\upsilon \rightarrow e^-_{(CB)} + h^+_{(VB)} \qquad (1)$$

When the irradiation is performed under vacuum the photoinduced charge carriers migrate in the crystal and a fraction of them can be stabilized at specific sites in the solid provided that the temperature is low enough to prevent electron-hole recombination. In such a case it is often possible to monitor by EPR the paramagnetic entities resulting from the described process. Photo-excited electrons are generally stabilized on metal cations, equation (2), forming, in most cases, shallow donor energetic levels just below the conduction band edge,

$$Me^{n+} + e^{-} \rightarrow \quad Me^{n-1} \qquad (2)$$

On the other hand, the photoinduced holes are stabilized at the oxygen ions of the lattice ($O_2^{\bullet-}$), producing the paramagnetic species $O^{\bullet-}$, equation (3):

$$O_2^{\bullet-} + h^{+}_{(VB)} \rightarrow O^{\bullet-} \qquad (3)$$

The g tensor of the $O^{\cdot-}$ ion ($2p_x^2, 2p_y^2, 2p_z^1$), has been reported by Brailsford. it shows, in general, a rhombic symmetry that, neglecting second order terms, becomes:

$$g_{zz} \sim g_e; \quad g_{xx} = g_e + 2\lambda/\Delta E_1 \,, g_{yy} = g_e + 2\lambda/\Delta E_2 \qquad (4)$$

where g_e is the free spin value (2.0023), λ is the spin-orbit coupling constant and ΔE_1 and ΔE_2 are the energy differences relating to the separation between $2p_z$ and the other two p-orbitals caused by the crystal field effect as shown in the scheme of Figure 5 [10-13].

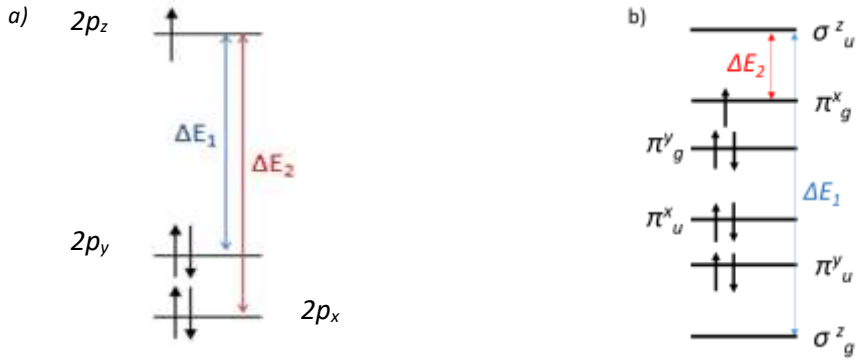

Figure 5: Crystal field effects on a: a) $O^{\cdot-}$ radical ion, b) $O_2^{\bullet-}$ radical ion.

The EPR signals of trapped electrons and trapped holes generally fall in distinct regions of the EPR spectrum, making easier the analysis of their stabilisation [14].

A further aspect of the EPR approach to the oxide photochemistry is the investigation of the interfacial reactivity of photogenerated charge carriers. In these case, irradiation is performed in the presence of a fluid phase (gas or liquid) in contact with the solid. In such a way the photo-induced charge carriers may react at the surface with molecules acting as scavengers of electrons and holes respectively. In general, if a surface electron transfer occurs, this lead to new paramagnetic entities that are monitored by EPR. The occurrence of this surface reactivity is, as a first approximation, the finger print of a mobility capable to lead the reactive charge at the surface, a preliminary condition for the occurrence of photocatalytic reactions. To evaluate the presence of photogenerated electrons at the surface, irradiation in O_2 atmosphere is performed leading to the formation of adsorbed superoxide radical anions ($O_2^{\bullet-}$) according to the following equation (5):

$$O_{2(gas)} + e^-_{(CB)} \rightarrow \quad O_2^{\bullet-}{}_{(ads)} \qquad (5)$$

The $O_2^{\bullet-}$ radical is characterized by un unpaired electron in a $2p\pi^*$ antibonding orbital, giving rise to a rhombic EPR signal with the following components [15, 16]:

$$g_{xx} = g_e \qquad (6)$$

$$g_{yy} = g_e + 2\lambda/E \qquad (7)$$

$$g_{zz} = g_e + 2\lambda/\Delta \qquad (8)$$

where Δ is the separation between the two $2p\pi^*$ orbitals of the absorbed superoxide species due to the electric field of the adsorption cationic site and E is the separation between the highest of the two $2p\pi^*$ orbitals and the $2p\sigma$ one. Considering that Δ is much smaller than E, the value of g_{zz} results to be very sensitive to the cation crystal field and is therefore diagnostic of the nature of surface site absorbing the $O_2^{\bullet-}$ ions [15].

The photoinduced holes can be stabilized at the solid surface by the oxide ions of the solid producing $O^{\bullet-}$ ions (equation 9)

$$h^+_{(VB)} + O_2^{\bullet-}{}_{(surf)} \rightarrow O^{\bullet-}{}_{(surf)} \qquad (9)$$

The formation of surface holes can be verified by irradiation in presence of H_2. This molecule reacts with $O^{\bullet-}$ undergoing a homolytic scission and generating reactive hydrogen atoms (eq. 10)

capable of injecting electrons into the material (eq. 11) that are usually stabilized at cationic sites in the lattice [17].

$$O^{\bullet-}_{(surf)} + H_2 \rightarrow OH^-_{(surf)} + H^\bullet \qquad (10)$$

$$H^\bullet + O_2^{\bullet-}{}_{(surf)} \rightarrow OH^-_{(surf)} + e^- \qquad (11)$$

In the case of heterogeneous photocatalytic reactions in aqueous media ROS are produced upon irradiation at the liquid-solid interface. The most important of these reactive species is the hydroxyl radical ($OH^\bullet$) produced by photo-induced holes (eq. 9) reacting with H_2O, equation (12), if the valence band (electro)chemical potential is more positive than that of water oxidation.

$$h^+_{(VB)} + H_2O \rightarrow OH^\bullet + H^+ \qquad (12)$$

Usually, the lifetime of OH radicals is too small to allow their direct detection by EPR. This issue can be bypassed using the spin trapping technique based on the reaction of the radical with a diamagnetic molecule (the trap) producing a stable paramagnetic adduct easily detected by EPR [18]. The most common spin trapping agents are aliphatic or cyclic nitrones such as the 5.5-dymethyl-1-pyrrolyne N oxide, also called DMPO, that reacting with $OH^\bullet$ radicals, forms the stable paramagnetic adduct shown in equation (13).

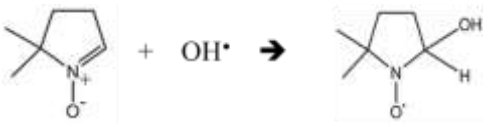

(13)

The $^\bullet$DMPO-OH paramagnetic adduct is characterized by the well-known EPR spectrum reported in Figure 6, whose structure is due to the hyperfine interaction of the unpaired electron with both ^{14}N (I = 1) and ^1H (I = 1/2) nuclei.

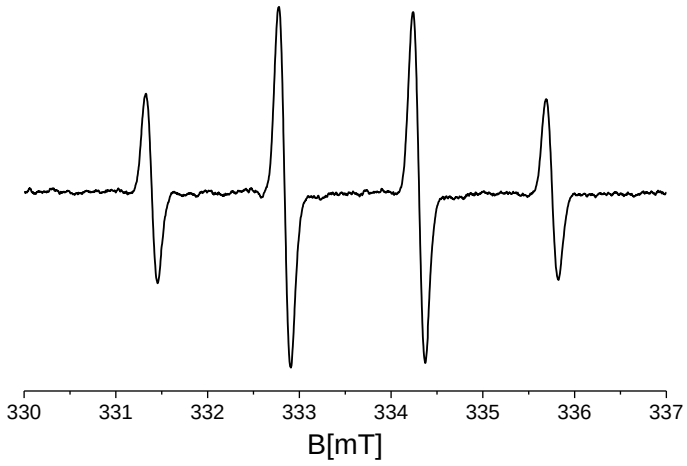

Figure 6: EPR spectrum of •DMPO-OH adduct.

To conclude, the EPR technique represents an efficient and valuable tool for the characterization of heterogeneous photocatalysts and, in particular, to perform preliminary screenings of the potentiality of new materials. In particular, EPR provides information on the basic photo-physical and photochemical properties of a given material.

In the following of this Chapter we will illustrate the role of EPR to characterize Visible Light Active (VLA) photocatalytic systems made up either by doped semiconducting oxides or by interfaced solid-solid systems.

N – TiO_2

Titanium dioxide, despite a band gap value corresponding to photons of the UV region, has been for many years the benchmark material for photocatalytic applications [19]. To extend its adsorption to the visible frequencies, much more abundant in the solar radiation, strategies based on doping the material have been proposed using either transition metal ions or, more recently, non-metallic elements such as carbon, sulphur and, with particular success, nitrogen. The first paper reporting the introduction of nitrogen species in TiO_2 was published in 1986 [20] and deals with the improved adsorption in the visible of N-doped TiO_2 but only after fifteen years it was released that this yellowish solid is active in photocatalytic reactions under visible light [20]. N-doped titania is usually prepared by sol-gel synthesis or by other wet-chemistry methods introducing a nitrogen containing substance in the reactants mixture.

The onset of photocatalytic activity under visible light was explained in terms of the presence of some nitrogen containing species in the bulk or at the surface of titania. An intense debate on the nature and structure of these centres started after the publications of the mentioned report characterized, [22] *inter alia*, by substantial contributions of EPR results, often coupled with DFT computational calculations.

The optical absorption of a typical N-TiO_2 system is shown in Figure 6, panel A, that compares the UV-vis diffuse reflectance spectroscopy (DRS) spectra of pristine and of nitrogen doped TiO_2 (anatase polymorph). Bare TiO_2 is characterized by the typical band gap transition at wavelengths lower than 400 nm while the nitrogen modified material shows an additional shoulder in the visible region, centred around 440 nm that explains its colour.

In parallel to this additional optical absorption it was found that doped TiO_2, reported in panel B of Figure 7, is also characterized by a EPR signal due to a previously unreported species containing nitrogen. The signal (Fig. 7, Panel B) is based on a hyperfine triplet indicating that the unpaired electron interacts with a single nucleus of ^{14}N (nuclear spin I = 1) and the corresponding species is photoactive since its intensity varies under irradiation.

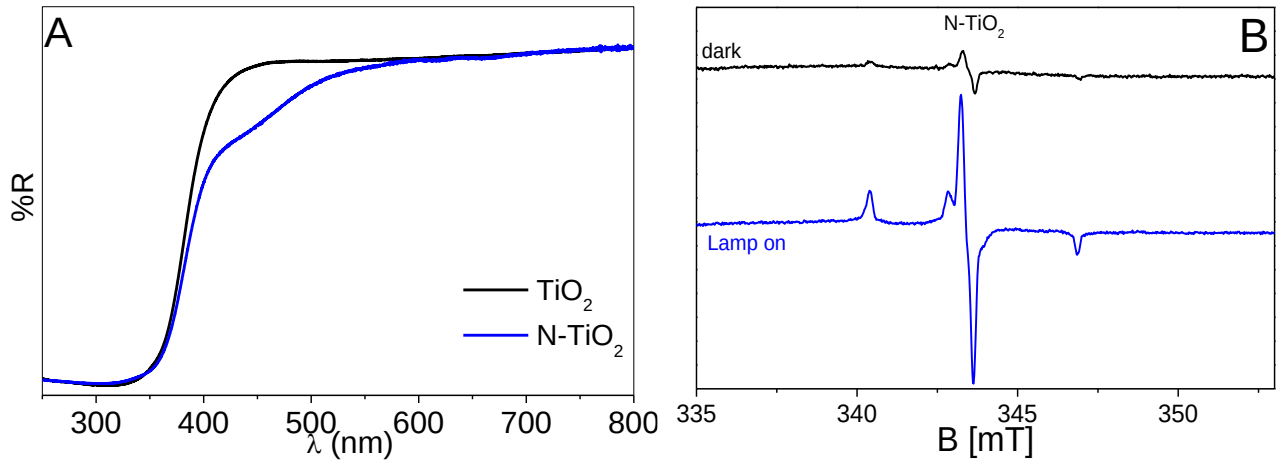

Figure 7. Panel A: UV-Vis DRS spectroscopy reflectance spectra of TiO_2 (black line) and N-TiO_2 (blue line). Panel B: EPR spectrum of N-TiO_2 before (black line) and after (blue line) irradiation with monochromatic light at λ = 440 nm in vacuum.

In particular, this occurs under blue light of about 440 nm corresponding to the maximum absorption in the visible. These EPR results, in strict connection with DFT calculations, have been

crucial to understand the nature and the features of the nitrogen defect. Actually, two types of photoactive centres have been described for N-TiO_2. The first one is based on substitutional nitrogen (N substitutes O in some lattice sites) and the second, more interesting from a photocatalysis standpoint, is preferentially formed using wet chemistry methods. It is based on a N atom positioned in an interstitial site of the structure and linked to a lattice O^{2-} thus forming a charged NO group in the bulk of the solid (formally $NO^{\bullet 2-}$). Beside this paramagnetic species, a diamagnetic one with two electrons in the HOMO is also present, that can be formally written as NO^{3-}. Both these chemical species correspond to intraband gap centres located few tenths of eV above the valence band edge that, as already mentioned, are responsible for the optical absorption in the visible of the doped system [23-25].

Figure 8 illustrates the photoactivity of the system under irradiation with monochromatic visible light (λ = 440 nm, blue) in oxygen atmosphere. In such conditions the EPR spectrum of a superoxide species absorbed at the surface on Ti^{4+} (g_{zz} = 2.028-2.023, g_{yy} = 2.009 and g_{xx} = 2.003) shows up (fig 8b) overlapping the signal of $NO^{\bullet 2-}$ (Fig. 8a) [23].

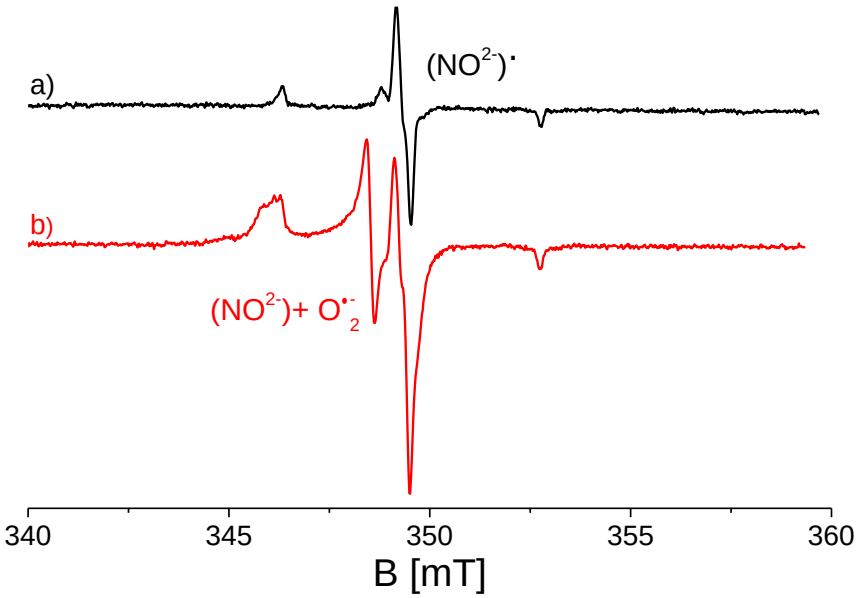

Figure 8: EPR spectra (77 K) of N-TiO_2 a) in the dark; b) after 1h of monochromatic visible irradiation (λ = 440 nm) in O_2. Adopted from ref. 26.

The formation of $O_2^{\bullet-}$ can be ascribed to the photo-excitation of electrons from the diamagnetic NO^{3-} centres to the TiO_2 conduction band (Eq. 14) with successive electron transfer to O_2 (Eq. 6). The additional $NO^{\bullet 2-}$ species generated by irradiation can be interpreted as a holes trapped at NO^{3-} sites

$$NO^{3-} + h\upsilon_{(\lambda=437nm)} \rightarrow NO^{\bullet 2-} + e^-_{(CB)} \qquad (14)$$

The formation of superoxide does not occur irradiating pristine TiO_2 under O_2 with the same type of light.

Fig. 9 displays the intensity decrease of the $NO^{\bullet 2-}$ signal upon NIR irradiation confirming occurrence the of photo-excitation from VB to the intra band gap $NO^{\bullet 2-}$ that are converted in the diamagnetic species NO^{3-}. The following equation (15) summarizes the phenomenon [26]:

$$e^-_{(VB)} + h\upsilon_{(\lambda=1550nm)} + NO^{\bullet 2-}_{(paramagnetic)} \rightarrow h^+_{(VB)} + NO^{3-}_{(diamagnetic)} \qquad (15)$$

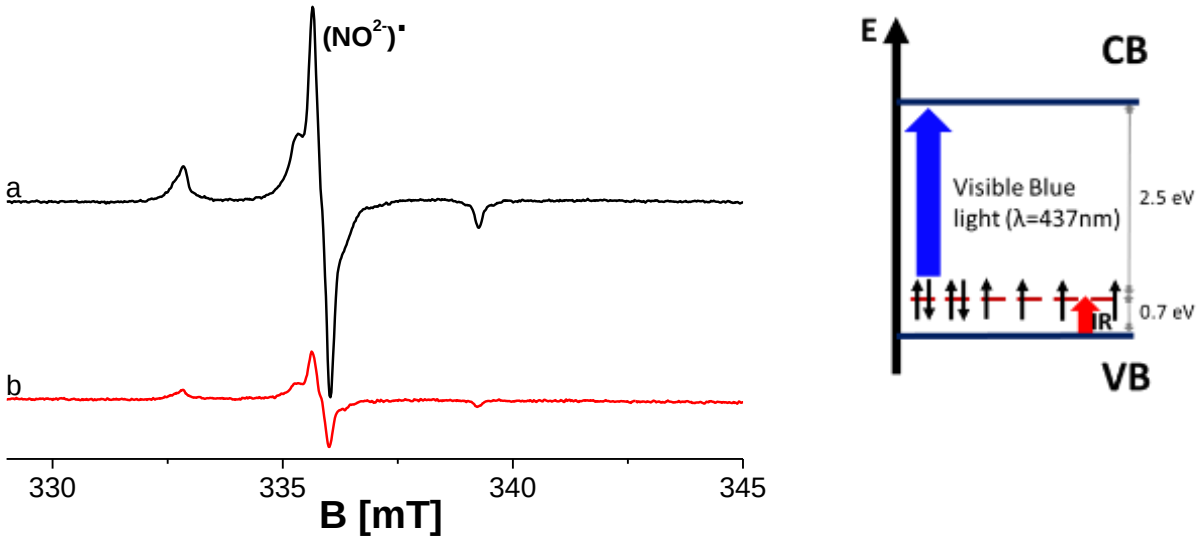

Figure 9. Left: EPR spectra (77 K) of N-TiO_2: a) in the dark (black line); b) during monochromatic IR light (λ = 1550 nm) in vacuum (red line). Adopted from ref. 27. Right: Schematic representation of the photoexcitation mechanisms observed in N-TiO_2 upon visible (437 nm) and IR (1550 nm) light irradiation

The effect of the processes in Eq. 14 and Eq.15 explains a possible mechanism of electron excitation from the VB to the CB by the combined effect of both NIR and visible photons. This mechanism, that confirms that N-TiO_2 is a true VLA system, has been unravelled by the joint use of EPR and specific monochromatic irradiations (Figure 9 right side).

Ce – ZrO_2

The case of cerium doped zirconium dioxide represents an attempt to use a large band gap semiconductor (ZrO_2, E_g= 5 eV, Fig. 10a)) in photocatalysis is order to exploit its favourable potentials for reductive and oxidative processes using however low energy photons in the process. This has been possible introducing Ce ions in the structure whose 4f empty levels act as a bridge to convey electrons from the VB to the CB using visible light. The resulting scheme reproduces a forecast by Emeline and Serpone who proposed a "third-generation" photocatalysts with this structure (Fig. 10b)) [27, 28].

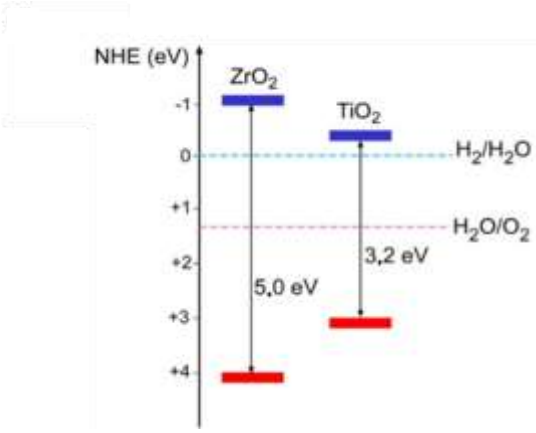

Figure 10: Relationship between the band structure of ZrO_2 and TiO_2 and redox potential of water splitting.

The addition of 0.5% moles of cerium ions (Ce^{4+}) to ZrO_2 is capable to completely overturn the optical and electronic properties of the bare oxide, converting it from a purely UV light sensitive material into a VLA system. The choice of rare-earth elements as doping source provides a unique opportunity, since their chemistry differs from that of the d-block metals. In particular, the *4f* orbitals, shielded by the more external $5s^2$ and $5p^6$ orbitals, don't directly take part in the bonding and form rather localized electronic states (see below).

The UV-vis spectra of Ce-doped and bare zirconia are compared in Figure 11.

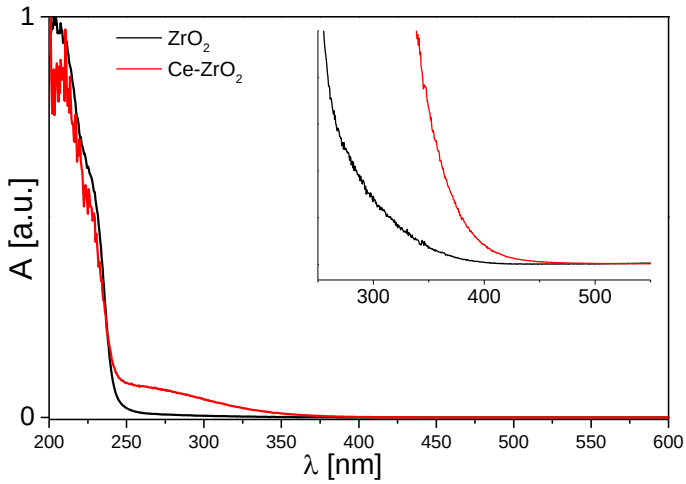

Figure 11: Normalized UV-vis absorption spectra of ZrO_2 (black line) and Ce-ZrO_2, 0.5% by moles (red line).

While the band gap transition of the pure oxide falls at 244 nm (5.08 eV), in the case of the doped material the absorption experiences a substantial red-shift with a weak absorption tail in the visible region. To better understand the effects of such weak visible absorption, EPR spectra have been recorded under irradiation with visible light having $\lambda \geq 420$ nm at 77 K and keeping the material under vacuum (Fig. 12) [29]. The sensitivity to visible light of the system shows up in terms of the formation of both trapped electrons and trapped hole EPR signals in such conditions. Electrons are trapped by Zr^{4+} ions that are reduced to Zr^{3+} (axial signal at high field with $g_{\parallel} = 1.977$ and $g_{\perp} = 1.959$) while trapped holes show the typical $O^{\bullet-}$ signal at low field (Figure 12) [30, 31]. This phenomenon has been interpreted, with the support of DFT calculations, in terms of the formation of mid-band gap Ce^{4+} 4f empty states. These permit a first step in the excitation conveying electrons from the valence band to the 4f states with low energy photons (about 2,5 eV). These excited electrons are, most likely, further promoted by a second photon to the conduction band of the system and stabilized at suitable Zr^{4+}sites [29].

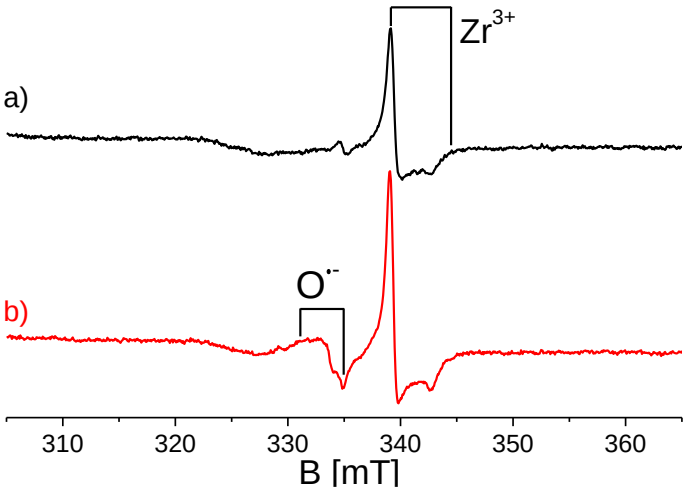

Figure 12: EPR spectra of Ce-ZrO_2 (0.5% cerium by moles) recorded at 77 K under vacuum: a) dark (black line, the material already contains trace of Zr^{3+} defects); b) irradiation having with polychromatic light $\lambda \geq 420$ nm (red line).

Like in the case of N-TiO_2, to verify the presence of reactive photoexcited carriers at the surface visible irradiations has been performed in the presence either of holes or of electrons scavengers (H_2 and O_2 respectively) according the Scheme illustrated in Section 3.

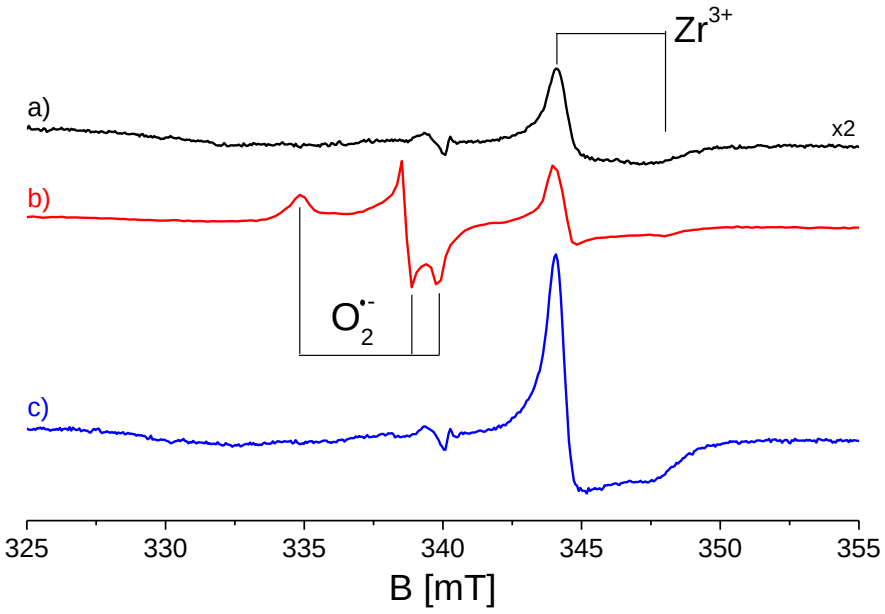

Figure 13: EPR spectra of Ce-ZrO_2 upon irradiation at 77 K with light having λ >420nm: a) background in dark (black line), b) in O_2 atmosphere (red line), c) in H_2 atmosphere (blue line).

As shown in Figure 13, visible light irradiation in oxygen atmosphere causes the formation of adsorbed superoxide according to Eq. 5 (Section 3). The same experiment performed in hydrogen

led to the formation of a further amount of Zr^{3+} ions (traces of Zr^{3+} defects are always present in the starting material) according to the complex process described in Eq. 10 and 11 ending up with the injection of an electron in the solid which is trapped by a Zr^{4+} ion. In short, the experiments illustrated in Figure 13 firmly point to the migration of reactive electron and holes at the surface of Ce-ZrO_2 irradiated with polychromatic visible light. Despite the relatively weak concentration of photogenerated surface charge carriers, that could actually limit the photocatalytic activity of the system, this result demonstrates that the insertion of Ce ions in ZrO_2 generate a VLA system which has shown appreciable photocatalytic activity in some practical applications of photocatalysis performed under visible irradiation [32-34]. DFT calculations corroborated these experimental results clarifying that the visible photo-sensibility of Ce-doped ZrO_2 is due to the incorporation of isovalent Ce^{4+} in the oxide lattice producing a series of unoccupied highly localized 4f levels in the middle of ZrO_2 band gap. As stated before these very levels are the bridge that allows the double electron transition described in Fig. 14 and reproducing the scheme proposed by Emeline and Serpone for photocatalysts of third generation.

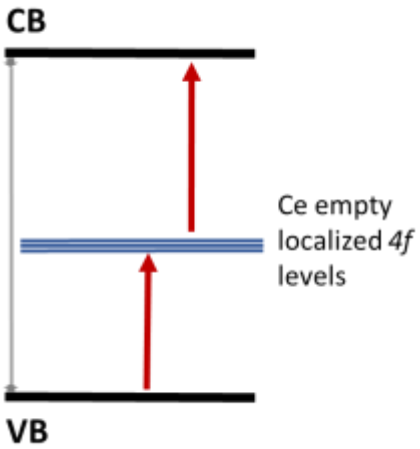

Figure 14: Two-step visible photons absorption mechanism of Ce-ZrO_2.

CeO_2 – ZnO

ZnO is a semiconducting oxide often considered in the past for photocatalytic applications despite of the fact that its band gap value (3.4 eV) requires the use of a UV light source for irradiation. At

variance with the previous case, there is no affinity between ZnO and CeO_2 that differ in terms of structure (wurtzite for ZnO and fluorite for CeO_2), ionic charge and size. The result of the combination of these two oxides is the formation of a heterogeneous system with dispersion of ceria nanocrystals on ZnO and the formation of a solid-solid heterojunction between the two components. Samples with ceria loading ranging between 1% and 10% have been prepared and tested by the described EPR-based procedure to preliminary investigate their photochemical behaviour [35-37].

TEM images, in Figure 15 show the presence of clustered colonies of ceria nanoparticles anchored at ZnO surfaces, confirming the presence of a biphasic system rather than a doped one.

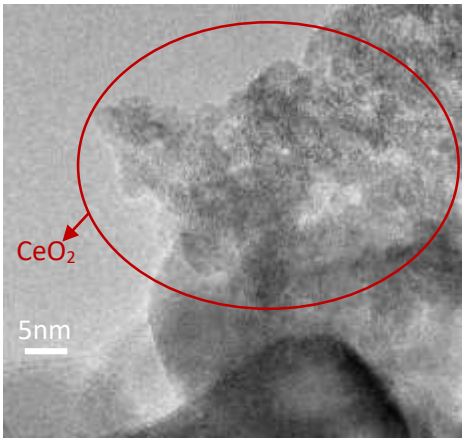

Figure 15: TEM image of CeO_2-ZnO.

EPR spectroscopy has been crucial in unravelling the VLA properties of the CeO_2/ZnO interface. Fig. 16 shows the spectrum of this hybrid system (Ce loading 1% by moles) recorded in the dark and showing the trace of tiny amounts of defects already present in the as-prepared material. These are due to trapped electron defects (g= 1.96, high field) corresponding to shallow electron donors always present in ZnO and likely generated by interstitial hydrogen impurities [38, 39] and to trapped holes ($O^{\bullet-}$ ions) visible in the low field portion of the EPR spectrum (Fig. 16a) respectively [10].

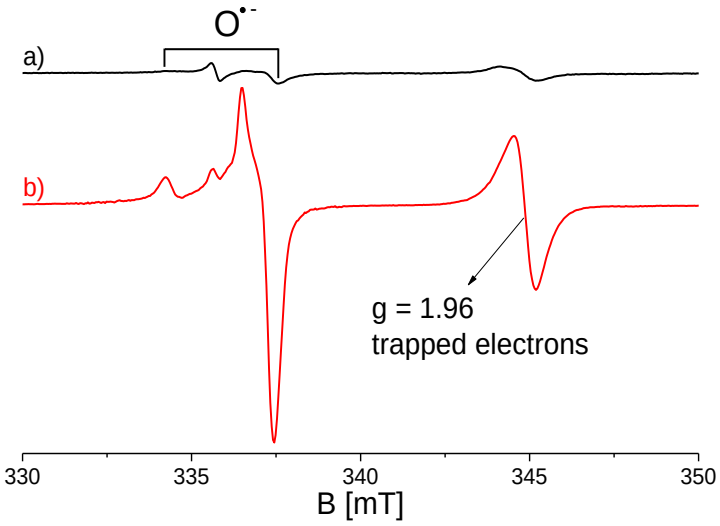

Figure 16: EPR spectra at 77K of CeO_2-ZnO in vacuum a) dark and (b) after irradiation with λ>420nm.

In spectrum b), recorded upon irradiation with polychromatic light having λ ≥ 420 nm under vacuum, both the trapped electron and trapped hole signals already present in the background markedly increase their intensity showing that a charge separation occurs in the system by the action of visible photons. The intensity increase of the trapped hole signal (Fig. 16b) is however higher than that of trapped electrons with g=1.96. This is caused by the fact that a fraction of the photoexcited electrons have been trapped by the cerium dioxide component forming reduced Ce^{3+} ions. These are

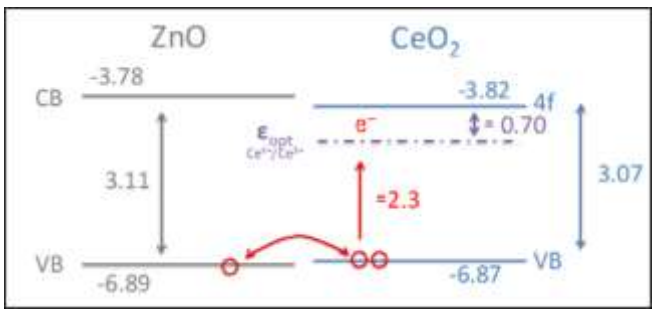

Figure 17: Schematic diagram of the final CeO_2-ZnO band alignment and the possible photoexcitation of the composite system. Values are reported in eV.

paramagnetic ions ([Xe]$4f^1$ configuration) however EPR silent since, due to the large value of the spin orbit coupling constant of the Ce atom, they are not visible in the conditions of the reported experiment (CW-EPR, 77K). A fraction of the photoformed electrons therefore escape detection so explaining the described intensity imbalance between the two signals in Fig. 16 [37]. Coupling EPR

data and DFT calculation, it has been possible to establish that the CeO_2-ZnO interface is a true visible-light-active heterojunction whose presence explains the reported results. Cerium dioxide is formally classified as insulator, since the gap between the valence band and the conduction band is about 6 eV; however empty, localized, *4f* levels of cerium are found almost 2.9 eV above the VB edge [40]. Theoretical calculations have shown that the VB of the two oxides have very similar flat band potential (Fig. 17). The *4f* levels of cerium, in the CeO_2-ZnO heterojunction, are thus located few tenths of eV below the ZnO conduction band limit. This allows an easy electronic transition from the conduction band of ZnO to the empty, localized, *4f* states of Ce^{4+}, forming partially reduced, EPR silent Ce^{3+}ions. The partial migration of photoexcited electrons on Ceria particles improves the spatial separation of the carriers thus favouring the photocatalytic effects.

As in the previously reported case, the surface activity of photo-promoted electrons and holes has been evaluated performing the visible irradiation under molecular oxygen and hydrogen atmospheres respectively, with the results reported in Figure 18, panel A and B. The formation of $O_2^{\bullet-}$ species absorbed on Zn^{2+} (g_{zz} = 2.049-2.055, g_{yy} = 2.009 and g_{xx} = 2.003 [15, 41, 42] and on Ce^{4+} ($g_{\perp}$=2.035 and $g_{\parallel}$=2.011 [43], confirms that the electrons, photo-excited by visible photons are able to migrate at the surface and to interact with both components of the hybrid system.

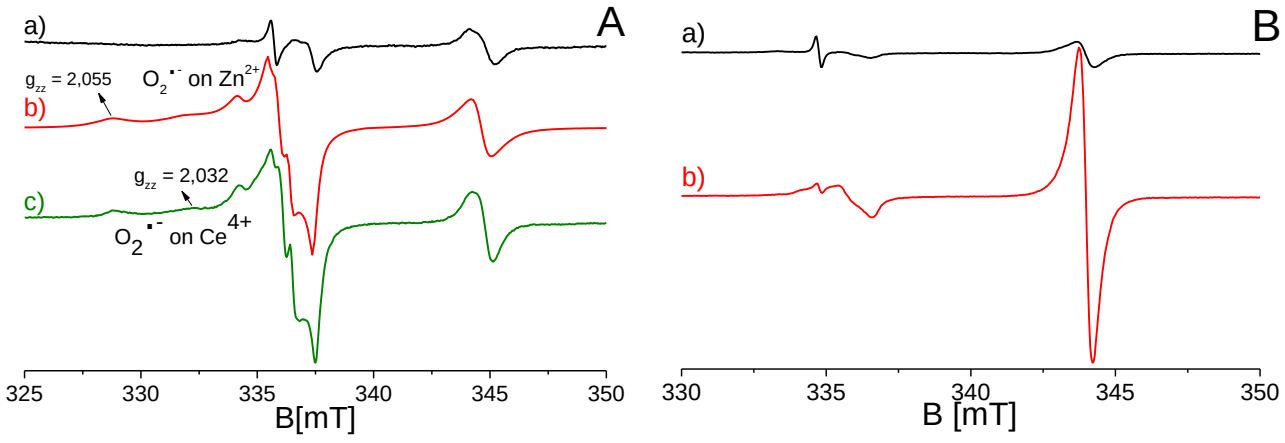

Figure 18: Panel A: EPR spectra at 77 K of CeO_2-ZnO: (a) background, spectrum in dark, (b) irradiation with visible light (λ > 420 nm) in the presence of molecular oxygen, (c) computer simulation of the whole spectrum b. Panel B: EPR spectra at 77 K of CeO_2-ZnO: (a) background, spectrum in dark, (b) irradiation with visible light (λ > 420 nm) in the presence of molecular hydrogen.

Also in the case of irradiation under hydrogen the result is extremely clear-cut since practically no trace of the trapped hole observed after irradiation under vacuum (Fig. 17) are now detected and only the signal at g = 1.96 growths in intensity to indicate the high efficiency of the surface reactivity of the photoformed holes according to the process described in Eq. 10 and Eq. 11.

The reactivity and the photo-oxidative ability of holes generated by visible light has been monitored also at the solid-liquid interface using the spin trapping technique, i.e. irradiating a CeO_2-ZnO aqueous suspension in presence of DMPO (see equation 12). Figure 19 reports the EPR trace of the •DMPO-OH adduct obtained by irradiation showing the propensity of the CeO_2-ZnO mixed material to form OH• radicals by the action of light having $\lambda \geq 420$ nm. The comparison with the same experiment performed using bare ZnO unambiguously clarify this effect.

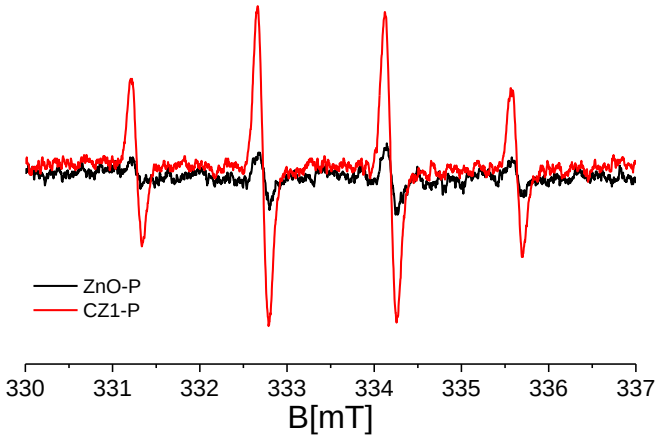

Figure 19. EPR spectra of the •DMPO/OH adduct produced by irradiation of an aqueous suspension of the CeO_2-ZnO (red line) and bare ZnO (black line) materials upon visible light ($\lambda \geq 420$ nm).

In conclusion, also for ZnO, the addition of a small amount of cerium gives rise to the formation of a photo-sensible material, where the intimate contact between the phases CeO_2 and ZnO is the cause of the visible light activity. The presence of CeO_2 and especially of the empty, localized *4f* states allows a beneficial charge carriers separation, with a fraction of photo-excited electrons stabilized on the defective cerium states. The described system, after the promising preliminary tests described above, was employed with good results in photocatalytic reactions for abatement of emerging pollutants such as acesulfame-K, iopamidol and bisphenol-A [44-46].

3. Conclusions

The present chapter has been devoted to describe the role played by Electron Paramagnetic Resonance to understand the photochemical and photophysical phenomena related to photocatalysis. This magnetic technique is extremely useful in performing preliminary tests aimed to verify the potentiality of newly produced photoactive systems. This is done by monitoring the photoinduced separation of charge carriers and their migration and reactivity at the surface in various conditions of irradiation. Particular attention has been paid to systems based on semiconducting oxides modified by doping in order to obtain visible light active (VLA) systems. The modifications considered consists in the insertion of heteroatoms in the oxide lattice like in the case of the well-known nitrogen doped titania (N-TiO_2) or in that of Ce-ZrO_2 forming intra band gap states that play a key-role in promoting excited electrons to the conduction band. It has also been shown that similar concepts apply in the case of a hybrid system made up by immiscible oxide like CeO_2 and ZnO that however form a particular solid-solid interface, or heterojunction, showing photoactivity under visible light similar to that observed in the case of doped materials.

Acknowledgment

Financial support from the Italian MIUR through the PRIN Project 20179337R7, MULTI-e "Multielectron transfer for the conversion of small molecules: an enabling technology for the chemical use of renewable energy" and the European Union's Horizon 2020 research and innovation programme under the Marie Skłodowska-Curie Grant Agreement No 765860 (AQUAlity) are gratefully acknowledge-edged.

References

[1] Cox, P. A., *Transition Metal Oxides: An Introduction to Their Electronic Structure and Properties*. OUP Oxford: 2010.

[2] D.F. Ollis, E. Pelizzetti, N. Serpone, Destruction of Water Contaminants, Environ. Sci. Technol. 25 (1991) 1522-29.

[3] M.R. Hoffman, S.T. Martin, W. Choi, D.W. Bahnemann, Environmental Applications of Semiconductor Photocatalysis, Chem. Rev. 95 (1995) 69-96.

[4] K. Maeda, K. Domen, Photocatalytic Water Splitting: Recent Progress and Future Challenges, J. Phys. Chem. Lett. 1 (2010) 2655-2661.
[5] A.B. Djurisic; Y.L. Leung; A.M.C. Ng, Strategies for Improving the Efficiency of Semiconductor Metal Oxide Photocatalysis. Mater. Horiz., 1 (2014) 400-410.
[6]. P. Zhou, J. Yu, M. Jaroniec, All-Solid-State Z-Scheme Photocatalytic Systems. Adv. Mater. 26 (2014) 4920-35.
[7] Y. Wang, Q. Wang, X. Zhan, F. Wang, M. Safdar, J. He, Visible light driven type II heterostructures and their enhanced photocatalysis properties: a review, Nanoscale 5 (2013) 8326-39.
[8] Q. Xu, L. Zhang, J. Yu, S. Wageh, A.A. Al-Ghamdi, M. Jaroniec, Direct Z-Scheme Photocatalysts: Principles, Synthesis, and Applications, Mater. Today 21 (2018) 1042-1063.
[9] D. Huang, S. Chen, G. Zeng, X. Gong, C. Zhou, M. Cheng, W. Xue, X. Yan, J. Li, Artificial Z-Scheme Photocatalytic System: What Have Been Done and Where to Go? Coord. Chem. Rev. 385 (2019) 44-80.
[10] M. Che, A.J. Tench, Characterization and Reactivity of Mononuclear Oxygen Species on Oxide Surfaces. Advances in Catalysis 31 (1982).
[11] C.D. Valentin, D. Ricci, G. Pacchioni, M. Chiesa, M.C. Paganini, E. Giamello, E., $O^{\bullet-}$ Radical Anions on Polycrystalline MgO., Surf. Sci. 521 (2002) 104-116.
[12] J.R. Brailsford, J.R. Morton, Paramagnetic Resonance Spectrum of O− Trapped in KCl, RbCl, and KBr. J. Chem. Phys. 51 (1969) 4794-4798.
[13] M. Chiesa, E. Giamello, C.D. Valentin, G. Pacchioni, The 17O hyperfine structure of trapped holes photo generated at the surface of polycrystalline MgO, Chem. Phys. Lett. 1-3 (2005) 124-128.
[14] M. Chiesa, M.C. Paganini, S. Livraghi, E. Giamello, Charge Trapping in TiO_2 Polymorphs as Seen by Electron Paramagnetic Resonance Spectroscopy. Phys. Chem. Chem. Phys. 15 (2013) 9435-47.
[15] M. Che, A.J. Tench, Characterization and Reactivity of Molecular Oxygen Species on Oxide Surfaces Adv. Catal. 32 (1983) 1-148.
[16] M. Chiesa, E. Giamello, M.C. Paganini, Z. Sojka, D.M. Murphy, Continuous Wave Electron Paramagnetic Resonance Investigation of the Hyperfine Structure of $^{17}O_2^-$ Adsorbed on the MgO Surface. J. Chem. Phys. 116 (2002) 4266-4274.
[17] T. Berger, O. Diwald, E. Knözinger, F. Napoli, M. Chiesa, E. Giamello, Hydrogen Activation at TiO_2 Anatase Nanocrystals. Chem. Phys. 339 (2007) 138-145.
[18] M.S. Jeong, K.N. Yu, H.H. Chung, S.J. Park, A.Y. Lee, M.R. Song, M.H. Cho, J.S. Kim, Methodological considerations of electron spin resonance spin trapping techniques for measuring reactive oxygen species generated from metal oxide nanomaterials. Scientific reports 6 (2016) 26347.
[19] D.A. Tryk, A. Fujishima, K. Honda, Recent topics in photoelectrochemistry: achievements and future prospects. Electrochim. Acta, 45 (2000) 2363-2376.
[20] S. Sato, Photocatalytic Activity of NO_X-doped TiO_2 in the Visible Light Region, Chem. Phys. Lett., 123 (1986) 126-128.
[21] R. Asahi, T. Morikawa, T. Ohwaki, K. Aoki, Y. Taga, Visible-Light Photocatalysis in Nitrogen-Doped Titanium Oxides, Science 293 (2001) 269-271.
[22] R. Asahi; T. Morikawa, T. Ohwaki, K. Aoki, Y. Taga, Visible-Light Photocatalysis in Nitrogen-Doped Titanium Oxides. Science 293 (2001) 269-271.
[23] S. Livraghi, M.C. Paganini, E. Giamello, A. Selloni, C.D. Valentin, G. Pacchioni, Origin of Photoactivity of Nitrogen-Doped Titanium Dioxide under Visible Light, J. Am. Chem. Soc. 128 (2006) 15666-15671.
[24] S. Livraghi, A. Votta, M.C. Paganini, E. Giamello, The nature of paramagnetic species in nitrogen doped TiO_2 active in visible light photocatalysis, Chem Commun (Camb) 4 (2005) 498-500.
[25] C. Di Valentin, G. Pacchioni, A. Selloni, S. Livraghi, E: Giamello, Characterization of Paramagnetic Species in N-Doped TiO_2 Powders by EPR Spectroscopy and DFT Calculations, J. Phys. Chem. Lett. 109 (2005) 11414-11419.
[26] G. Barolo, S. Livraghi, M. Chiesa, M.C. Paganini, E. Giamello, Mechanism of the Photoactivity under Visible Light of N-Doped Titanium Dioxide. Charge Carriers Migration in Irradiated N-TiO_2 Investigated by Electron Paramagnetic Resonance, J. Phys. Chem. C 116 (2012) 20887-20894.
[27] N. Serpone, A.V. Emeline, Semiconductor Photocatalysis - Past, Present, and Future Outlook. J. Phys. Chem. Lett. 3 (2012) 673-7.

[28] A.V. Emeline, V.N. Kuznetsov, V.K. Ryabchuk, N. Serpone, On the way to the creation of next generation photoactive materials, Environ Sci Pollut Res Int., 19 (2012) 3666-75.
[29] C. Gionco, M.C. Paganini, E. Giamello, R: Burgess, C. Di Valentin, G. Pacchioni, Cerium-Doped Zirconium Dioxide, a Visible-Light-Sensitive Photoactive Material of Third Generation, J. Phys. Chem. Lett. 5 (2014) 447-51.
[30] C. Morterra, E. Giamello, L. Orio, M. Volante, Formation and Reactivity of Zr^{3+} Centers at the Surface of Vacuum-Activated Monoclinic Zirconia, J. Phys. Chem., 94 (1990) 3111-3116.
[31] C. Gionco, M.C. Paganini, E. Giamello, R. Burgess, C. Di Valentin, G. Pacchioni, Paramagnetic Defects in Polycrystalline Zirconia: An EPR and DFT Study, Chem. Mater., 25 (2013) 2243-2253.
[32] C. Gionco, M.C: Paganini, E. Giamello, O. Sacco, V. Vaiano, D. Sannino, Rare Earth Oxides in Zirconium Dioxide: How to Turn a Wide Band Gap Metal Oxide into a Visible Light Active Photocatalyst. J. Energy Chem. 26 (2016) 270-276.
[33] C. Gionco, S. Hernández, M. Castellino, T.A. Gadhi, J.A. Muñoz-Tabares, E. Cerrato, A. Tagliaferro, N. Russo, M.C. Paganini, Synthesis and Characterization of Ce and Er doped ZrO_2 Nanoparticles as Solar Light Driven Photocatalysts, J. Alloys Compd., 775 (2019) 896-904.
[34] F.E. Bortot Coelho, C. Gionco, M.C: Paganini, P. Calza, G. Magnacca, Control of Membrane Fouling in Organics Filtration Using Ce-Doped Zirconia and Visible Light. Nanomaterials 9 (2019).
[35] E. Cerrato, C. Gionco, M.C. Paganini, E. Giamello, Photoactivity Properties of ZnO Doped with Cerium Ions: an EPR Study, J. Phys. Condens. Matter., 29 (2017) 1-7.
[36] E. Cerrato, C. Gionco, I. Berruti, F. Sordello, P. Calza, M.c. Paganini, Rare earth ions doped ZnO: Synthesis, characterization and preliminary photoactivity assessment. J. Solid State Chem., 264 (2018) 42-47.
[37] E. Cerrato, C. Gionco, M.C. Paganini, E. Giamello, E. Albanese, G. Pacchioni, Origin of Visible Light Photoactivity of the CeO_2/ZnO Heterojunction, ACS Appl. Energy Mat., 1 (2018) 4247-4260.
[38] E. Cerrato, M.C. Paganini, E. Giamello, Photoactivity under visible light of defective ZnO investigated by EPR spectroscopy and photoluminescence, J. Photochem. Photobiol. A, 397 (2020) 112531.
[39] A. Janotti, C.G. Van de Walle, New insights into the role of native point defects in ZnO, J. Cryst. Growth, 287 (2006) 58-65.
[40] E. Wuilloud; B. Delley; D. Schneider; Y. Baer, Spectroscopic Evidence for Localized and Extended f-Symmetry States in CeO_2. Phys. Rev. Lett., 53 (1984) 202-205.
[41] M. Iwamoto, Y. Yoda, N. Yamazoe, T. Seiyama, Study of Metal Oxide Catalysts by Temperature Programmed Desorption. Oxygen Adsorption on Various Metal Oxides, J. Phys. Chem., 82 (1978) 2564-2570.
[42] R.D. Iyengar; Rao, V. V. S.; A.C. Zettlemoyer, ESR Studies of the Interaction of O_2, NO_2, N_2O, NO and Cl_2 with Zinc Oxide, Surf. Sci., 13 (1969) 251-262.
[43] M. Che, J.F.J. Kibblewhite, A.J. Tench, M. Dufaux, C. Naccache, Oxygen Species Adsorbed on CeO_2/SiO_2 Supported Catalysts, J. Chem. Soc., Faraday Trans., 69 (1973) 857-863.
[44] P. Calza, C. Gionco, M. Giletta, M. Kalaboka, V.A. Sakkas, T. Albanis, M.C. Paganini, Assessment of the Abatement of Acelsulfame K Using Cerium Doped ZnO as Photocatalyst, J. Hazard. Mater., 323 (2016) 471-477.
[45] M.C. Paganini, D. Dalmasso, C. Gionco, V. Polliotto, L. Mantilleri, P. Calza, P., Beyond TiO_2: Cerium-Doped Zinc Oxide as a New Photocatalyst for the Photodegradation of Persistent Pollutants, Chem. Select, 1 (2016) 3377-3383.
[46] O. Bechambi, L. Jlaiel, W. Najjar, S. Sayadi, Photocatalytic Degradation of Bisphenol A in the Presence of Ce-ZnO: Evolution of Kinetics, Toxicity and Photodegradation Mechanism, Mater. Chem. Phys., 173 (2016) 95-105.